Clays and Clay Minerals, Vol. 61, No. 2, 133–140, 2013.

QUANTITATIVE *IN SITU* STUDY OF THE DEHYDRATION OF BENTONITE-BONDED MOLDING SANDS

GUNTRAM JORDAN[1], CONSTANZE EULENKAMP[1], ELBIO CALZADA[2], BURKHARD SCHILLINGER[2], MARKUS HOELZEL[2], ALEXANDER GIGLER[1], HELGE STANJEK[3], AND WOLFGANG W. SCHMAHL[1]

[1] Ludwig-Maximilians-Universität München, Department für Geo- und Umweltwissenschaften, Theresienstr. 41, 80333 München, Germany

[2] Technische Universität München, FRM II, Lichtenbergstr.1, 85748 Garching, Germany

[3] RWTH Aachen, Ton- und Grenzflächenmineralogie, Wüllnerstr. 2, 52065 Aachen, Germany

Abstract—Bentonite-bonded molding sand is one of the most common mold materials used in metal casting. The high casting temperatures cause dehydration and alteration of the molding sand, thereby degrading its reusability. Neutron radiography and neutron diffraction were applied to study these processes by using pure bentonite-quartz-water mixtures in simulation casting experiments. The aim of the experiments was to compare the dehydration behavior of raw and recycled mold material in order to assess possible causes of the limited reusability of molding sands in industrial application. Neutron radiography provided quantitative data for the local water concentrations within the mold material as a function of time and temperature. Dehydration zones, condensation zones, and areas of pristine hydrated molding sand could be established clearly. The kinematics of the zones was quantified. Within four cycles of de- and rehydration, no significant differences in water kinematics were detected. The data, therefore, suggest that the industrial handling (molding-sand additives and the presence of metal melt) may have greater effects on molding-sand reusability than the intrinsic properties of the pure bentonite–quartz–water system.

Key Words—Bentonite, Dehydration Process, Metal Casting, Molding Sand, Neutron Powder Diffraction, Neutron Radiography, Smectite.

INTRODUCTION

Large quantities of casted metal parts are produced with bentonite-bonded molding sands. Smectite, as the main component of bentonite, provides the required binding properties. Binding is partially related to the negative layer charge of the smectites. In the interlayer space, cations compensate for the layer charge. These interlayer cations can hydrate reversibly, resulting in a swelling of the interlayer space. X-ray powder diffractometry (XRD) revealed the dependence of the d_{001} value on the interlayer hydration states (*e.g.* Bradley *et al*., 1937; Ferrage *et al*., 2005a, 2005b; Moore and Reynolds, 1997; Norrish, 1954). The uptake and release of water is influenced by various factors such as size, valence, hydration energy of the interlayer cation, and the charge, as well as the charge distribution of the layers (Collins *et al*., 1992; Ferrage *et al*., 2005b, 2007c; Jasmund and Lagaly, 1993; Koster van Groos and Guggenheim, 1984). Furthermore, hydration takes place discontinuously and different hydration states can coexist within an interlayer (Aldushin *et al*., 2007; Ben Brahim *et al*., 1984; Bérend *et al*., 1995; Cases *et al*., 1997; Collins *et al*., 1992; Sánchez-Pastor *et al*., 2010; Wilson *et al*., 2004). Analogously, dehydration occurs discontinuously. Investigations by XRD (Ferrage *et al*., 2007a, 2007b) showed that Ca-montmorillonite evolves during drying from one hydration state to another *via* mixed-layer structures. Thermogravimetric analysis (Bray and Redfern, 1999; El-Barawy *et al*., 1986; Guggenheim and Koster van Groos, 2001; Koster van Groos and Guggenheim, 1984; Zabat and Van Damme, 2000) showed that dehydration takes place in the range 50−350ºC depending on the experimental conditions. Bray and Redfern (1999) reported a two-step dehydration where adsorbed water was released before interlayer water. Guggenheim and Koster van Groos (1992, 2001) demonstrated that water fugacity influences the dehydration of smectites to a great extent. According to these authors, water adsorbed at surfaces plays a major role in dehydration below 100ºC. Compaction of the sample, in contrast, gained importance above 100ºC.

Although smectites have been investigated intensively, the dehydration and rehydration kinetics on an industrial scale of both pure smectite and of mold materials are not understood sufficiently. While isothermal uptake and release of interlayer water is generally considered to be a reversible process, the occurrence of sorption-desorption-hysteresis clearly indicates complex kinetics (*e.g.* Cases *et al*., 1992; Komadel *et al*., 2002). Furthermore, any alterations of the chemical state of the layers (*e.g.* Wu *et al*., 1989) or elevated temperatures (*e.g.* Ferrage *et al*., 2007a) can cause irreversible modifications of de- and rehydration behavior.

* E-mail address of corresponding author:
guntram.jordan@lrz.uni-muenchen.de
DOI: 10.1346/CCMN.2013.0610210

Industrially processed mold material loses its capability to reabsorb water (Grefhorst *et al*., 2005; Tilch, 2004). This limits considerably the reusability of the material. As a consequence, only 93–98 wt.% of the mold material is recycled after casting. Environmental aspects as well as the demands of increasing production efficiency, however, require an increased reusability rate for molding sand. A detailed understanding of the uptake and release of water in mold material is, therefore, essential.

The aim of the present study was to better understand the limitations of the reusability of molding sands in industrial applications. In order to accomplish this goal, multi-cycle experiments were performed which simulated the recurring thermal impact of industrial-scale casting on a pure quartz-bentonite-water system. The application of the pure system enabled discrimination between potential effects originating from intrinsic mineral properties (*e.g*. reversible *vs*. irreversible dehydration of smectites) and actual industrial handling (*e.g*. alterations of the mold material by the metal melt or additives such as reducing agents). Information on the spatial and temporal distribution of water within the mold material during thermal impacts was obtained by applying neutron radiography (*cf.* Fijal-Kirejczyk *et al*., 2011; Luo, 2007) and neutron powder diffractometry.

SAMPLES AND METHODS

Samples

Additive-free molding sand with a compactibility of 45–50% was obtained from S&B Industrial Minerals GmbH (Marl, Germany). The composition of the molding sand was 84 wt.% quartz sand (average grain size 0.24 mm; Frechen, Germany), 12 wt.% sodium bentonite (Wyoming, USA), and 3–4 wt.% water. The composition of the bentonite was calculated from XRD data using the software package *BGMN* (Ufer *et al*., 2008): 87 wt.% montmorillonite, 4 wt.% quartz, 4 wt.% albite, 2 wt.% muscovite, 2 wt.% calcite, 1 wt.% brookite.

Casting simulation experiment

A container (approx. size 140 mm × 67 mm × 60 mm) was filled with molding sand and equipped with thermocouples located at heights of ~0, 10, 20, 30, 40, and 50 mm (Figure 1a). The container was mounted in an experimental stand at the neutron imaging facility ANTARES (FRM II, Germany; Schillinger *et al*., 2006) and dropped onto a preheated hotplate (~650ºC; Figure 1b) while taking neutron radiographs (2048 × 2048 pixel CCD camera, 2 × 2 binning mode, spatial sample resolution ~0.15 mm). The temperature of the hotplate was chosen in order to avoid massive dehydroxylation of smectites progressing far into the bulk molding sand. In order to facilitate constant thermal conditions in the beam direction, low heat flow from the copper-baseplate to the front and rear aluminum walls of the container was desirable. The front and rear walls, therefore, were mounted at a distance of 3 mm from the baseplate of the container. Thus, the container had a 3 mm wide slit at the bottom edges between the baseplate and the front and rear walls. The radiograph acquisition frequency was ~0.21 Hz which determined the temporal resolution of the experiments. The neutron radiography observations lasted for ~24 min. A detailed description of the experimental set-up can be found in Schillinger *et al*. (2011).

The water lost by the dehydration experiments was determined gravimetrically. De-ionized water was then added to the dehydrated sand. Due to the limited accuracy of the gravimetric determination (~0.1% of the total mass of sand and container), the mass of added water varied in multi-cyclic experiments by up to ~10%. The re-moistened molding sand was homogenized with a blender for ~5 min. The sand was then left undisturbed in a plastic bag for 3 days (the possibility of water loss during this period cannot be excluded completely). In all experiments, loading of the container and compaction of the sand were conducted in a standardized way to ensure maximum homogeneity and the best possible reproducibility.

Neutron radiography contrast

Attenuation of the neutron beam by transmission through the mold container from its initial intensity, I_0, to intensity I can be described by:

$$I/I_0 = \exp\left(-\sum_i \delta_i x_i\right) \quad (1)$$

where δ_i is the attenuation coefficient of the phase i, and x_i is the partial path length of the neutron beam passing through phase i with $x_i = a_i\, x$ (where a_i is the partial length coefficient and x is the beam-path length of the entire mold container).

Because neutron attenuation depends on the amount of hydrogen in the beam path, the hydration state of the molding sand can be correlated directly to the neutron intensity detected by the CCD camera. The sum in equation 1, therefore, can be split into one term for the mold container filled with dehydrated molding sand (s) and a second term accounting for water (w). The logarithm of equation 1 then yields:

$$\ln(I/I_0) = -\delta_s x_s - \delta_w x_w \quad (2)$$

Converting the radiography detector signal into linearly normalized grayscales (GS_n) between unity for the open beam without any sample ($I = I_0$; $GS_{n\ \text{open beam}} = 1 = I/I_0$) and zero for the beam shut off ($I = I/I_0 = 0$; $GS_{n\ \text{dark image}} = 0$), equation 2 yields:

$$\ln(GS_n) = -\delta_s x_s - \delta_w x_w \quad (3)$$

For the normalized grayscales in a dehydrated reference radiograph ($GS_{n\ \text{dehydr}}$), the last term vanishes:

https://doi.org/10.1346/CCMN.2013.0610210 Published online by Cambridge University Press

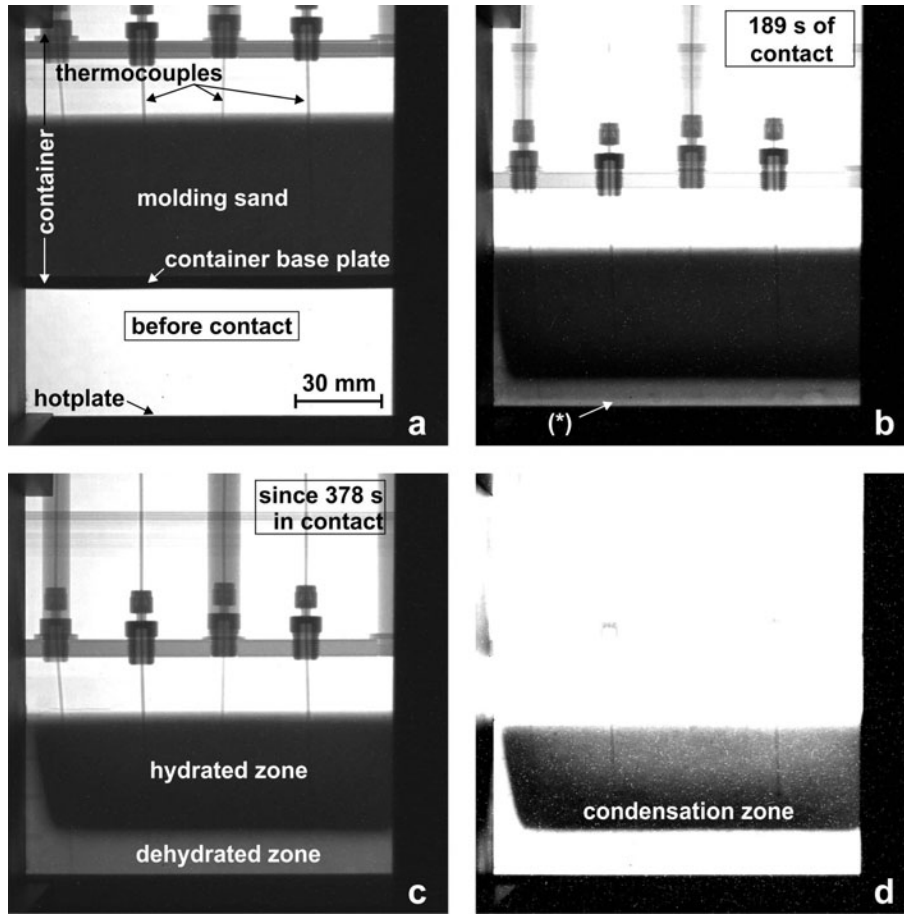

Figure 1. Neutron radiographs of a casting simulation experiment. Image grayscales are a measure of the neutron scattering intensity. Changes in the intensity essentially correlate with changes in the local concentration of water. (a) Radiograph shows the molding-sand container (equipped with thermocouples) ~45 mm above the hotplate. (b) The container has been in contact with the hotplate for 189 s. The molding sand in the lowest region of the container is dehydrated. (c) A further 189 s later the vertical extent of the dehydrated zone has grown significantly. (d) Same radiograph as in part c with adjusted brightness and contrast settings. The modified settings allow the identification of a condensation zone located in the lower range of the hydrated zone.

$$\ln(GS_{n\ \mathrm{dehydr}}) = -\delta_s x_s \tag{4}$$

Combining equations 3 and 4 yields:

$$x_w = \frac{\ln(GS_{n\ \mathrm{dehydr}}) - \ln(GS_n)}{\delta_w} \tag{5}$$

Taking into account a neutron attenuation coefficient for water $\delta_w = 5.415\ \mathrm{cm}^{-1}$ (www.ncnr.nist.gov with $\lambda = 4$ Å) and the bulk density of the molding material (obtained from the weight and fill level of the container), equation 5 permits determination of the wt.% of water of the molding material displayed in the radiographs within the above-mentioned limits of spatial and temporal resolution.

Note, however, that the incident neutron beam is not mono-energetic but has a spectrum mostly ranging from 1.8 to 6 Å, centered around 3.5–4 Å. In addition, the tabulated attenuation coefficient treats scattering like absorption (*i.e.* scattered neutrons do not reach the detector) and does not account for forward-scattered neutrons that hit the large detector area under small angles, leading to a diffuse background. The additional absolute error may well be up to ~15%, but cannot be quantified without extensive numerical simulations. However, comparing the conditions of this study (x_w < 3 mm for the fully hydrated molding sand; sample–detector distance >5 cm) with the scattering profiles obtained by Hassanein (2006), no significant contribution of scattered neutrons in the radiographs was expected. Furthermore, at a neutron transmission below ~15%, multiple scattering may affect the accuracy of the quantification of absolute water contents to some extent. The accuracy of equation 5, therefore, decreases with increasing mold-container thickness and increasing water content. The molding sand used in the experiments yielded transmissions ranging from ~8% (fully hydrated) to ~30% (dehydrated). The experiments below, however,

https://doi.org/10.1346/CCMN.2013.0610210 Published online by Cambridge University Press

compare relative measurements under very similar conditions.

Neutron powder diffraction

In order to identify different hydration states of smectite by an evaluation of the position and intensity of the 001 peak, neutron powder diffraction was conducted using the thermal high-resolution neutron powder diffractometer SPODI (FRM II, Germany; Hoelzel *et al*., 2012). The molding sand (mass ~5 g) was analyzed in its original state, after dehydration in the casting simulation experiment, and after rehydration. All neutron diffraction measurements were performed at room temperature and wavelengths λ = 2.396 Å or 2.536 Å using a germanium (331) monochromator at take-off angles of 135º or 155º, respectively. A possible λ/3 contribution was avoided by a graphite filter. The positions of the 001 peaks in the diffraction patterns have been verified by applying the Rietveld refinement program *BGMN* which uses a fundamental parameter approach to model the peak profiles (Ufer *et al*., 2004). For the instrumental resolution function of SPODI, a width formula for a single squared Lorentzian was used.

RESULTS

Casting simulations

Neutron radiography recorded the temporal and spatial intensity variations of the neutron beam passing through the mold-sand container during the experimental casting simulation. Because hydrogen fluxes are controlling these intensity variations almost exclusively, dehydration processes and water fluxes could be accessed directly and quantitatively.

Neutron radiographs were taken from the mold-sand container in contact with a hotplate underneath (Figure 1b). A 3 mm zone of significant dehydration (recognizable by lighter grayscales) initiated at the bottom of the container (asterisk in Figure 1b). This zone was caused by rapid venting of water vapor through the 3 mm slits between the front and rear walls and the baseplate of the container (see above). With increasing residence time of the container on the hotplate (Figure 1c), dehydration of the molding sand continued upwards. Dehydrated molding sand in the lower region and hydrated sand on top were easily distinguished visually. Modified brightness and contrast settings of the detector data (*cf.* Figure 1c,d) also revealed an increased amount of water in the lower range of the hydrated sand region.

The normalized detector data (GS_n) were taken along vertical profiles of the mold container (profile data point = mean value from a horizontal 1 × 330 pixel strip). The profile data were converted into water-concentration profiles by applying equation 5 and using the density of the mold material in the container. The mean grayscale of the most dehydrated parts of the sand in the last three images of the radiograph sequence was used as a reference value for $GS_{n\ \mathrm{dehydr}}$. Thermocouples placed in this area indicated a temperature range of 200−250ºC. The radiographs did not give any indication of a dehydroxylation reaction in these areas. Water concentration profiles (Figure 2a) were obtained from radiographs of dehydrating raw molding sand (first dehydration) and of molding sand that has been de- and rehydrated four times before (Figure 2b).

The hydration states at the locations of two different thermocouples (2 and 3 cm above the container baseplate) were plotted *vs*. the corresponding temperature readings of the thermocouples for the two different molding sands (Figure 3). Assuming that water was the only mobile component in the system, the plots can be perceived as local thermo-gravimetric measurements within larger sample systems. Note that these local measurements also revealed reallocations of water within a sample, whereas standard thermo-gravimetric analyses integrated over the entire sample volume and measured only the net escape of water from a system. Furthermore, due to the non-linearity of the local heating rate, the temperature scales of such plots (Figure 3) did not correspond to a linear time scale. The water contents *vs*. temperature plots (Figure 3) revealed the general behavior of an initial increase in water concentration, followed by a decrease above ~100ºC. Time-synchronization errors of radiography and temperature data logging limited the precision of the determination of the transition point between hydration and dehydration.

Neutron diffractometry

Neutron powder diffractometry of raw molding sand revealed smectite d_{001} values of ~19 Å (Figure 4). After dehydration in the experimental casting simulation stand, the molding sand was measured again. A smectite d_{001} value of 9.7 Å was observed. Subsequently, the molding sand was rehydrated by adding the gravimetrically determined amount of lost water and a resting period of 3 days. The sand revealed smectite d_{001} values of ~19 Å again.

A second set of diffractometry experiments focused on rehydration kinetics. After dehydration of the molding sand, the lost water was determined gravimetrically and re-added. The sand was then homogenized and left undisturbed for ~30 min. Subsequently, diffraction patterns were taken every 90 min over a period of 8.5 h. The water uptake of smectite interlayers was monitored by the position of the 001 reflection of smectite. The d_{001} value expanded to ~19 Å within 2.5 h and remained constant thereafter (Figure 5).

DISCUSSION

Different hydration states of smectite interlayers result in different d_{001} values (*e.g.* Couture, 1985; Ferrage *et al*., 2005a, 2005b; Jasmund and Lagaly,

https://doi.org/10.1346/CCMN.2013.0610210 Published online by Cambridge University Press

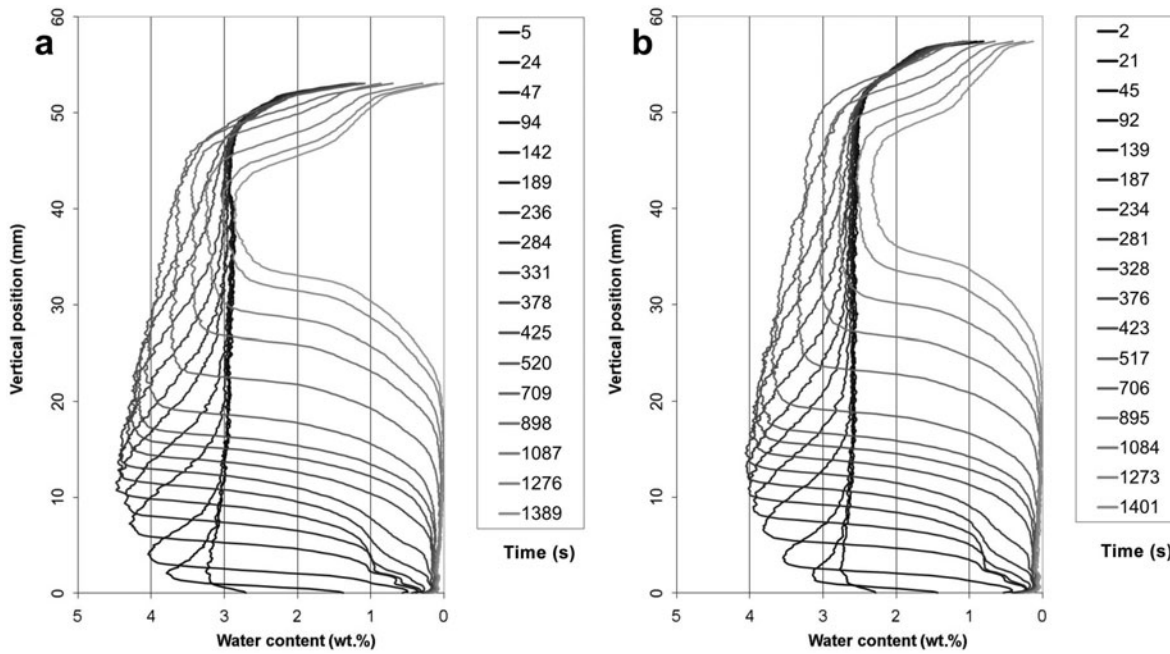

Figure 2. Evolution of the water concentration profiles in a raw molding sand (a) and a recycled molding sand (b) during the casting simulation experiment. The water concentrations were converted from the grayscales taken over the entire vertical extent of the molding-sand container obtained at given times in the respective radiograph.

1993; Wilson *et al*., 2004). Non-hydrated Na- and Ca-smectites have d_{001} values of 9.6−10.1 Å. Mono- and bi-hydrated smectites show 12.3−12.7 Å and 15.1−15.8 Å, respectively. The uptake of three water layers leads to d_{001} values of 19−20 Å. Identification of the hydration states of smectite in molding sand was made possible by neutron powder diffraction in spite of the small amount, 12 wt.%. Smectites in raw molding sand showed d_{001} values of ~19 Å (Figures 4 and 5) which correspond to smectite interlayers with three water layers (Wilson *et al*., 2004). This indicates that the smectite interlayers in the raw molding sand used for casting simulation were fully hydrated.

After the heat treatment, the molding sand was extracted from the casting simulation apparatus and analyzed by neutron diffractometry. The d_{001} values decreased to ~9.7 Å, which indicates complete dehydration. This result was confirmed by Ferrage *et al*. (2007a) who observed a transition from mono- to dehydrated Ca-montmorillonite at temperatures >90ºC. The authors further report that the relative abundance of dehydrated interlayers was ~70% after 950 s at 125ºC. Complete dehydration was predicted to occur at ~170ºC.

After the dehydration experiments, the amount of water lost was determined gravimetrically and was re-added to the dehydrated molding sand. Neutron diffractometry (Figures 4 and 5) showed that the smectite d_{001} values increased to ~19 Å (corresponding to three water layers) within 2.5 h. Therefore, the smectites of recycled molding sand used in subsequent dehydration experiments (Figure 2b) had had the same hydration state as pristine molding sand. Note, however, that due to small differences in the shape of the d_{001} peak, hydration heterogeneities within the smectites cannot be discounted completely.

The formation of three water layers within 2.5 h contradicts the statement of Dieng (2005) who reported rehydration of pores within ~1 h and of interlayers within a day or more. Although the compositions of the samples used by Dieng (2005) were not fully defined, the smectite contents (25−97%) were substantially greater than the 12 wt.% used here. A possible dependence of the hydration state of the smectites on the porosity (and, therefore, of the water transport capacity of the samples) cannot be excluded.

Comparing the neutron radiographs of raw and recycled molding sand (*cf*. Figure 2), the general process of dehydration was identical. Within the limits of temporal resolution of radiography, the release of water started instantaneously upon contact of container and hotplate. Initially, water vapor migrated in two directions: it rose and re-condensed in the still colder zone above and it vented through the slits between baseplate and container walls. The larger the dehydrated zone grew, the less water vented through the base slits. After ~300 s, the amount of water venting through the slits was negligible and upward transport to the condensation zone took place exclusively. After ~700 s, water concentration profiles were considerably influenced by the fill level of molding sand in the container.

The maximum local water concentration correlated with a temperature of ~100ºC (Figure 3). With increas-

https://doi.org/10.1346/CCMN.2013.0610210 Published online by Cambridge University Press

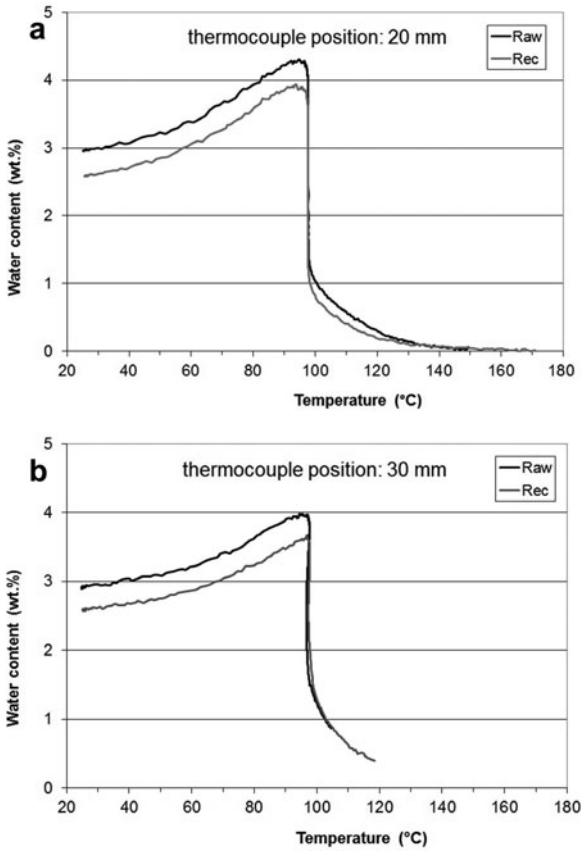

Figure 3. Plots of water concentrations obtained from the radiographs during an entire casting simulation experiment at the position of a thermocouple *vs*. the related temperature reading. For better comparison, the plots of raw (Raw) and recycled (Rec) molding sands were grouped for the thermocouples located 20 mm (a) and 30 mm (b) above the base plate.

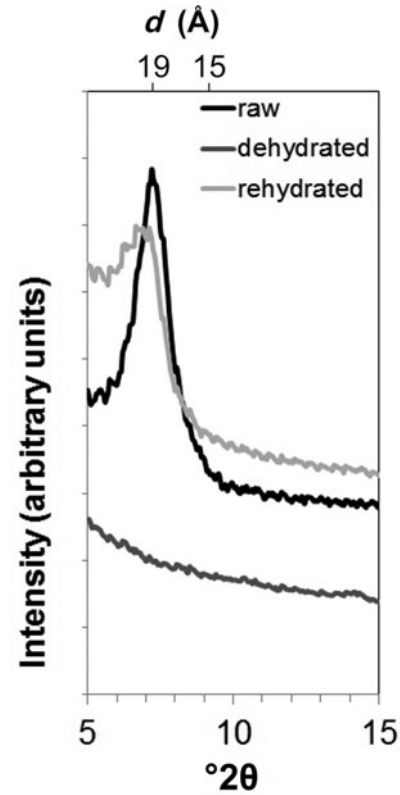

Figure 4. 001 reflection of smectites in neutron powder diffraction patterns (λ = 2.396 Å) of molding sands. The raw and rehydrated molding sands have similar d_{001} values of ~19 Å. The diffractogram of dehydrated molding sand shows a peak with very weak intensity at ~14.2°2θ yielding a *d* value of ~9.7 Å. The intensities were normalized to the incident neutron counts.

ing temperature, the water concentration reduced rapidly. Subsequently, the dehydration rate decreased continuously until dehydration ceased in the temperature range 170–220ºC. Above 100ºC, neither the vertical profiles (Figure 2) nor the plots of local water concentrations *vs*. temperature (Figure 3) revealed any sign of an onset of a new process associated with a noticeable release of hydrogen. Within the period of radiographic observation, no indication of a dehydroxylation of the octahedral sheets of smectite was, therefore, observed. However, the possibility that thermal treatment caused a chemical alteration of some smectites which may have led to a modified re-hydration behavior of these minerals cannot be ruled out. Irreversible dehydration taking place at temperatures above 90ºC was reported by Ferrage *et al*. (2007a).

Irrespective of any possible alteration of the smectites, all water lost from the molding sand by the casting simulation was re-added within the accuracy of the gravimetric measurement. A potential deficit of water within the interlayers would result in a surplus of pore water. Therefore, the observed differences in the initial water concentrations of the raw and recycled molding sand (Figure 3) cannot be associated with a reduced capacity of smectites to reabsorb water but rather with the limited accuracy of the water-loss measurement.

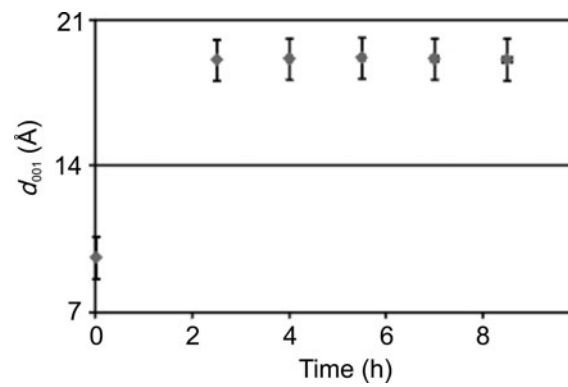

Figure 5. Neutron powder diffraction data of rehydrating molding sand. The d_{001} values of smectite were plotted *vs*. the rehydration time. The *d* values were verified using the Rietveld program code *BGMN*.

https://doi.org/10.1346/CCMN.2013.0610210 Published online by Cambridge University Press

An important point of the casting simulation experiment is that, prior to any dehydration, molding sand first and foremost is subject to a hydration process within the condensation zone at temperatures up to 100ºC. Whether these hot-hydrous conditions lead to a rapid hydration of a few still dehydrated interlayers (which may be present in some smectites) or whether the hot-hydrous conditions (rather than the subsequent hot-dry conditions) are more likely to alter the chemical state of smectites and to reduce their de- and rehydration capacity is unknown. In bentonite samples at least, steam has been identified to efficiently reduce the swelling capacity (Couture, 1985).

Irrespective of the effects of the condensation zone, neutron diffractometry showed that the smectite interlayers in all casting simulation experiments were hydrated and that the concentration of chemically modified smectites, if present at all, was below the detection limit. The only obvious difference between the raw and recycled molding sand directly prior to the onset of dehydration at ~100ºC, therefore, is pore-water concentration. For temperatures above 100ºC, Guggenheim and Koster van Groos (2001) suggested that dehydration kinetics of surface-adsorbed water may be controlled by sand compaction rather than binding affinity. This may also hold for pore water. A correlation between molding-sand compaction and dehydration kinetics can be expected and may explain the observed similar dehydration behavior of raw and recycled molding sand.

CONCLUSIONS

The kinetics of dehydration of the pure quartz-bentonite-water system in the casting simulation experiments performed here was probably controlled by the compaction of the material. Due to similar compaction of the molding sand used here, the dehydration kinetics of both raw and recycled molding sand revealed no significant difference. Further experiments should, therefore, focus on small-scale variations of water contents and its distribution kinetics within a porous system, where diffusional transport might be much more important relative to mechanical mixing.

If the casting simulation experiments caused irreversible alterations of smectites, the effects of these alterations on the dehydration kinetics were insignificant within the number of cycles performed. The occurrence of fast and significant reduction of molding-sand binding properties by industrial handling, therefore, seems more likely to be a consequence of the industrial handling (*e.g.* alterations by the metal melt or additives) rather than originating from naturally intrinsic mineral properties (*e.g.* irreversibility of smectite dehydration). The application of neutron radiography, *e.g.* to additive-containing moldings sands, could help to identify the main cause of the loss of quality of the molding sand.

ACKNOWLEDGMENTS

Help with the Rietveld refinement program *BGMN* provided by the late Jörg Bergmann is gratefully acknowledged. Molding-sand samples were kindly provided by S&B Industrial Minerals GmbH. The work was supported financially by the BMBF/DFG Sonderprogramm Geotechnologien (Forschungsvorhaben 03G0707). The comments provided by the Editor in Chief, the Associate Editor, and two anonymous reviewers improved the manuscript considerably and are gratefully acknowledged.

REFERENCES

Aldushin, K., Jordan, G., Aldushina, E., and Schmahl, W.W. (2007) On the kinetics of ion-exchange in phlogopite – an *in situ* AFM study. *Clays and Clay Minerals*, **55**, 339–347.

Ben Brahim, J., Besson, G., and Tchoubar, C. (1984) Etude des profils des bandes de diffraction X d'une beidellite-Na hydratée à deux couches d'eau. Détermination du mode d'empilement des feuillets et des sites occupés par l'eau. *Journal of Applied Crystallography*, **17**, 179–188.

Bérend, I., Cases, J.M., Francois, M., Uriot, J.P., Michot, L., Masion, A., and Thomas, F. (1995) Mechanism of adsorption and desorption of water vapor by homoionic montmorillonite: 2. The Li^+, Na^+, K^+, Rb^+ and Cs^+ exchanged forms. *Clays and Clay Minerals*, **43**, 324–336.

Bradley, W.F., Grim, R.E., and Clark, G.F. (1937) A study of the behavior of montmorillonite upon wetting. *Zeitschrift für Kristallographie*, **97**, 260–270.

Bray, H.J. and Redfern, S.A.T. (1999) Kinetics of dehydration of Ca-montmorillonite. *Physics and Chemistry of Minerals*, **26**, 591–600.

Cases, J.M., Bérend, I., Besson, G., Francois, M., Uriot, J.-P., Thomas, F., and Poirier, J. (1992) Mechanism of adsorption and desorption of water vapor by homoinonic montmorillonite. 1. The sodium-exchanged form. *Langmuir*, **8**, 2730–2739.

Cases, J.M., Bérend, I., Francois, M., Uriot, J.P., Michot, L.J., and Thomas, F. (1997) Mechanism of adsorption and desorption of water vapor by homoionic montmorillonite: 3. The Mg^{2+}, Ca^{2+}, Sr^{2+} and Ba^{2+} exchanged forms. *Clays and Clay Minerals*, **45**, 8–22.

Collins, D.R., Fitch, A.N., and Catlow, C.R. (1992) Dehydration of vermiculite and montmorillonite: A time resolved powder neutron diffraction study. *Journal of Materials Chemistry*, **2**, 865–873.

Couture, R. (1985) Steam rapidly reduces the swelling capacity of bentonite. *Nature*, **318**, 50–52.

Dieng, M.A. (2005) Der Wasseraufnahmeversuch nach DIN 18132 in einem neu entwickelten Gerät. *Bautechnik*, **82**, 28–32.

El-Barawy, K.A., Girgis, B.S., and Felix, N.S. (1986) Thermals treatment of some pure smectites. *Thermochimica Acta*, **98**, 181–189.

Ferrage, E., Lanson, B., Malikova, N., Plançon, A., Sakharov., B.A., and Drits, V.A. (2005a) New insights on the distribution of interlayer water in Bi-hydrated smectite from X-ray profile modeling of 00l reflections. *Chemistry of Materials*, **17**, 3499–3512.

Ferrage, E., Lanson, B., Sakharov. B.A., and Drits, V.A. (2005b) Investigation of smectite hydration properties by modeling of X-ray diffraction patterns: Part I. Montmorillonite hydration properties. *American Mineralogist*, **90**, 1358–1374.

Ferrage, E., Kirk, C., Cressey, G., and Cuadros, J. (2007a) Dehydration of Ca-montmorillonite at the crystal scale. Part 1. Structure evolution. *American Mineralogist*, **92**, 994–1006.

Ferrage, E., Kirk, C., Cressey, G., and Cuadros, J. (2007b) Dehydration of Ca-montmorillonite at the crystal scale. Part 2. Mechanisms and kinetics. *American Mineralogist*, **92**, 1007–1017.

Ferrage, E., Lanson, B., Sakharov, B.A., Geoffroy, N., Jacquot, E., and Drits, V.A. (2007c) Investigation of dioctahedral smectite hydration properties by modeling of X-ray diffraction profiles: Influence of layer charge and charge location. *American Mineralogist*, **92**, 1731–1743.

Fijal-Kirejczyk, I.M., Milczarek, J.J., and Zoladek-Nowak, J. (2011) Neutron radiography observations of inner wet region in drying of quartz sand cylinder. *Nuclear Instruments and Methods in Physics Research A*, **651**, 205–210.

Grefhorst, C., Podobed, O., and Böhnke, S. (2005) Bentonitgebundene Formstoffe: Umlaufverhalten von Bentoniten unter besonderer Betrachtung des Kreislaufsystems und der Nasszugfestigkeit. *Gießerei*, **92**, 63–67.

Guggenheim, S. and Koster van Groos, A.F. (1992) High-pressure differential thermal analysis (HP-DTA). I. Dehydration reactions at elevated pressures in phyllosilicates. *Journal of Thermal Analysis*, **38**, 1701–1728.

Guggenheim, S. and Koster van Groos, A.F. (2001) Baseline studies of the Clay Minerals Society Source Clays: thermal analysis. *Clays and Clay Minerals*, **49**, 433–443.

Hassanein, R.K. (2006) Correction methods for the quantitative evaluation of thermal neutron tomography. PhD dissertation No 16809, ETH Zürich, Switzerland, 102 pp.

Hoelzel, M., Senyshyn, A., Juenke, N., Boysen, H., Schmahl, W., and Fuess, H. (2012) High-resolution neutron powder diffractometer SPODI at research reactor FRM II. *Nuclear Instruments and Methods in Physics Research A*, **667**, 32–37.

Jasmund, K. and Lagaly, G. (editors) (1993) *Tonminerale und Tone*. Steinkopff Verlag, Darmstadt, Germany.

Komadel, P., Hrobáriková, J., Smrčok, L., and Koppelhuber-Bitschnau, B. (2002) Hydration of reduced-charge montmorillonite. *Clay Minerals*, **37**, 543–550.

Koster van Groos, A.F. and Guggenheim, S. (1984) The effect of pressure on the dehydration reaction of interlayer water in Na-montmorillonite (SWy-1). *American Mineralogist*, **69**, 872–876.

Luo, X. (2007) Study of infrastructure materials using neutron radiography and diffraction. PhD dissertation, University of Tennessee, Knoxville, USA, 192 pp.

Moore, D.M. and Reynolds, R.C. Jr. (1997) *X-ray Diffraction and Identification and Analysis of Clay Minerals*. Oxford University Press, Oxford, UK and New York.

Norrish, N. (1954) The swelling of montmorillonite. *Discussions of the Faraday Society*, **18**, 120–133.

Sánchez-Pastor, N., Aldushin, K., Jordan, G., and Schmahl, W.W. (2010) K^+-Na^+ exchange in phlogopite on the scale of a single layer. *Geochimica et Cosmochimica Acta*, **74**, 1954–1962.

Schillinger, B., Calzada, E., and Lorenz, K. (2006) Modern neutron imaging: Radiography, tomography, dynamic and phase contrast imaging with neutrons. *Solid State Phenomena*, **112**, 61–72.

Schillinger, B., Calzada, E., Eulenkamp, C., Jordan, G., and Schmahl, W.W. (2011) Dehydration of moulding sand in simulated casting process examined with neutron radiography. *Nuclear Instruments and Methods in Physics Research A*, **651**, 312–314.

Tilch, W. (2004) Ermittlung des Aufbereitungsverhaltens bentonitgebundener Formstoffe (Betriebssande). *Gießerei-Praxis*, **1/2004**, 12–18.

Ufer, K., Roth, G., Kleeberg, R., Stanjek, H., Dohrmann, R., and Bergmann, J. (2004) Description of X-ray powder pattern of turbostratically disordered layer structures with a Rietveld compatible approach. *Zeitschrift für Kristallographie*, **219**, 519–527.

Ufer, K., Stanjek, H., Roth, G., Dohrmann, R., Kleeberg, R., and Kaufholf, S. (2008) Quantitative phase analysis of bentonites by the Rietveld method. *Clays and Clay Minerals*, **56**, 272–282.

Wilson, J., Cuardros, J., and Cressey, G. (2004) An *in situ* time-resolved XRD-PSD investigation into Na-montmorillonite interlayer and particle rearrangement during dehydration. *Clays and Clay Minerals*, **52**, 180–191.

Wu, J., Low, P.F., and Roth, C.B. (1989) Effects of octahedral-iron reduction and swelling pressure on interlayer distances in Na-nontronite. *Clays and Clay Minerals*, **37**, 211–218.

Zabat, M. and Van Damme, H. (2000) Evaluation of the energy barrier for dehydration of homoionic (Li, Na, Cs, Mg, Ca, Ba, $Al_x(OH)_y^{z+}$ and La)-montmorillonite by a differentiation method. *Clay Minerals*, **35**, 357–363.

(*Received 22 November 2012; revised 7 March 2013; Ms. 728; AE: S. Kadir*)